LAWRENCE
LIVERMORE
NATIONAL
LABORATORY

LLNL-JRNL-781432

Understanding the effects of radiative preheat and self-emission from shock heating on equation of state measurement at 100's of Mbar using spherically converging shock waves in a NIF hohlraum

J. Nilsen, A. L. Kritcher, M. E. Martin, R. E. Tipton, H. D. Whitley, D. C. Swift, T. Doppner, B. L. Bachmann, A. E. Lazicki, N. B. Kostinski, B. R. Maddox, G. W. Collins, S. H. Glenzer, R. W. Falcone

July 15, 2019

Matter and Radiation at Extremes

Disclaimer

This document was prepared as an account of work sponsored by an agency of the United States government. Neither the United States government nor Lawrence Livermore National Security, LLC, nor any of their employees makes any warranty, expressed or implied, or assumes any legal liability or responsibility for the accuracy, completeness, or usefulness of any information, apparatus, product, or process disclosed, or represents that its use would not infringe privately owned rights. Reference herein to any specific commercial product, process, or service by trade name, trademark, manufacturer, or otherwise does not necessarily constitute or imply its endorsement, recommendation, or favoring by the United States government or Lawrence Livermore National Security, LLC. The views and opinions of authors expressed herein do not necessarily state or reflect those of the United States government or Lawrence Livermore National Security, LLC, and shall not be used for advertising or product endorsement purposes.

Understanding the effects of radiative preheat and self-emission from shock heating on equation of state measurement at 100's of Mbar using spherically converging shock waves in a NIF hohlraum

Joseph Nilsen[1], Andrea L. Kritcher[1], Madison E. Martin[1], Robert E. Tipton[1], Heather D. Whitley[1], Damian C. Swift[1], Tilo Döppner[1], Benjamin L. Bachmann[1], Amy E. Lazicki[1], Natalie B. Kostinski[1], Brian R. Maddox[1], Gilbert W. Collins[2], Siegfried H. Glenzer[3], and Roger W. Falcone[4]

[1]Lawrence Livermore National Laboratory, Livermore, CA 94551
[2]University of Rochester, Rochester, NY 14627
[3]SLAC National Accelerator, Menlo Park, CA 94025
[4]University of California Berkeley, Berkeley, CA 94720

Abstract. Over the last six years many experiments have been done at the National Ignition Facility to measure the Hugoniot of materials such as plastic at extreme pressures from 20 - 800 Mbar. The "Gbar" design employs a strong spherically converging shock launched through a solid ball of material using a hohlraum radiation drive. The shock front conditions are characterized using X-ray radiography. In this paper we examine the role of radiation in heating the un-shocked material in front of the shock to understand the impact this has on the EOS measurements and how this drives the measured data off the theoretical Hugoniot curve. In particular the two main sources of radiation heating are the preheat of the un-shocked material from the high energy keV X-rays in the hohlraum and the heating of the material in front of the shock as the shocked material becomes hot enough to radiate significantly. We show how the preheat can reach 4 eV in the unshocked material and the radiation heating can start driving the data significantly off the Hugoniot at pressures above 400 Mb.

1. Introduction

Laboratory measurements of matter at high energy density is of great importance in understanding the structure and evolution of astrophysical objects such as gas-giant planets, brown dwarfs, and highly evolved stars material where extreme pressures can exceed 100 Mbar and reach well into the Gbar regime. [1-3] At Lawrence Livermore National Laboratory (LLNL) the Gbar experimental platform has been developed and demonstrated [4-6] to study the shock compression (Hugoniot) of material compressed to near Gbar pressures in a spherically converging geometry using streaked X-ray radiography. In these experiments, the National Ignition Facility (NIF) laser heats the inside of a gold hohlraum and creates an X-ray radiation drive which ablates an outer ablator and sends a strong spherical shock into a solid sphere of material. The shock velocity and the density jump at the shock front are characterized using X-ray radiography to determine the pressure and density along the shock Hugoniot as the shock travels to the center of the solid sphere. As the shock travels toward the center the pressure increases like ~1/r and the temperature at the shock front increases, accordingly. Eventually this leads to strong X-ray self-emission, which heats

the un-shocked material in front of the shock and changes the assumption used in the Hugoniot equations that the unshocked material is cold. Recent experiments have measured the Hugoniot of CH plastic from 20 – 60 Mbar in a low-drive (300 kJ) NIF experiment [5,6] while other experiments have measured the Hugoniot from 100 – 400 Mbar in a high-drive (1.1 MJ) NIF experiments. [7] In this paper we look at the two sources of radiation heating for the unshocked material and the effect this heating has on the interpretation of the Hugoniot measurement. In addition to the X-ray self-emission at the shock front we also examine the role of the target being preheated by the high energy keV X-rays from the hohlraum. We will show in this paper that preheating is not an issue for the low-drive NIF experiments that measure data from 40 – 130 Mbar but can effectively heat the targets to several eV and put the experiment on a slightly different Hugoniot for the high-drive Gbar experiments that measure 100's of Mbar. We will also show that the self-emission from the shock front limits the pressure we can measure on the Hugoniot to about 400 Mbar in the case of plastic even though the experiment measures data up to 800 Mbar.

2. Gbar experimental platform to measure Hugoniot EOS data

The Gbar experimental platform is described in more detail in Refs. 4-7 but we give a brief overview of the recent experiments to measure the EOS of poly(α-methylstyrene) C_9H_{10} plastic at pressures from 20 – 400 Mbar. A schematic of the experimental configuration is shown in Fig. 1(a). A more detailed description of the experiment can be found in Ref. 5. In these experiments, solid targets are compressed and heated in an indirect drive laser geometry using 176 laser beams incident on an Au hohlraum. The targets consisted of solid CH spheres 970 μm in radius covered by a 185 μm thick plastic ablator made of glow-discharge polymer (GDP) with a graded Ge (Z=32) dopant. The Ge dopant serves as both a marker layer in the experiment for the radiography as well as a preheat shield to reduce preheat of the plastic target. The ablator consisted of four layers as shown in detail in Fig. 1. The second layer, which is 33 μm thick, is doped with 1.1% Ge by atomic fraction and served as the primary marker layer and preheat shield.

The experiments use a standard NIC scale 5.75 mm hohlraum (diameter = 5.75 mm and height = 9.42 mm) with a 0.03 mg/cc ^{4}He gas fill and 3.375 mm diameter laser entrance hole. The hohlraum is driven by 176, 351-nm laser beams. For the low-drive experiments [5,6] the pulse shape is a 4-ns long, nearly square pulse with power of 78 TW while the high-drive experiments [7] use a two shock pulse shape that can be described as an 1-ns duration, 75-TW initial square

pulse that then ramps up to 330 TW over 2-ns and maintains 330 TW over the next 2-ns [7]. The total drive energy and power incident on the hohlraum walls is about ≅ 300 kJ for the low-drive experiments and 1.2 MJ for the high drive experiments. These drive conditions result in a predicted peak hohlraum radiation temperature near 200 eV for the low-drive and 300 eV for the high drive experiments. In both cases the idea is to drive a single strong shock through the plastic target and measure a locus of Hugoniot points as the shock propagates through the target.

3. Radiation hydrodynamic simulations

In this section we present radiation hydrodynamics design simulations to model and understand the EOS measurements using the Gbar platform and the sensitivity of the experiments to radiation preheat and self-emission from the shock front. To simplify the simulations, we changed the material slightly in the modeling to be pure polystyrene, CH, at a density of 1.05 g/cc. These simulations are capsule-only simulations that use a frequency dependent (FDS) radiation source that surrounds the capsule. This drive is derived from integrated Hohlraum simulations using a Detailed Configuration Accounting (DCA) atomic physics model [8]. This radiation drive was modified to account for the fact that 16 of the 192 drive beams are used to drive the back-lighter for the streaked radiography. The radiation temperature as a function of time is plotted in Fig. 2 for the low-drive and high-drive experiments. The peak radiation temperature is predicted to be 191 and 286 eV for the low and high-drive experiments, respectively. To model this in one-dimension (1D) the simulations are done using the LASNEX radiation-hydrodynamic code [9]. The average-atom based tabular equation-of-state (EOS) table LEOS 5400 is used for the CH sphere and LEOS 5358 for the doped GDP ablator. The radiation transport is modeled using Sn multi-group radiation transport [10,11] with 110 radiation groups. To resolve the shock front the simulations use 0.25 μm zoning across the entire CH sphere.

For the low-drive experiment, the simulations predict that the ablation pressure at the boundary of the CH peaks at 41 Mbar at a time of 4.7 ns. The shock continues to travel inward and starts to slowly increase as it reaches a radius of 600 μm around 8.85 ns. To understand how to extract Hugoniot data from the simulations we developed a shock tracking routine that starts at the center of the calculation and looks for the first peak in the entropy. This gives us the location of the rising-edge of the incoming shock front. We then examine the pressure in adjacent zones and test that the pressure is not changing by more than 1% from zone to zone and define this as the location of the

shock. We have tried other methods such as looking for the spatial derivative of the pressure to fall to 1-3% of its peak value and gotten very similar results for the location of the shock front. In Fig. 3 we plot the shock pressure vs position of the shock front. Table 1 shows how the pressure starts near 39 Mbar when the shock is at a radius of 600 μm and slowly increase to 73 Mb at a radius of 200 μm. Between radii of 200 and 100 μm the pressure climbs more rapidly from 73 to 132 Mb as the shock reaches 100 μm at t=14.96 ns. Experimentally it becomes hard to measure the shock with adequate resolution below a radius of 100 μm as the shock continues to accelerate inward to the center. Figure 4 shows the pressure and density vs radius when the shock is at radii of 500 and 200 μm. At a radius of 500 μm the density and pressure both peak at the shock front and it is easy to extract the plasma parameters at the shock front. As the radius decreases the pressure increase slightly while the density increases significantly behind the shock front which is why the shock tracking routines needs to look at derivatives in the pressure to identify the shock front. This pileup of the density behind the shock front is characteristic of the converging geometry.

Reference 6 gives a detailed description of how the Hugoniot data is extracted from the radiographic data in the low-drive NIF experiments. The Rankine-Hugoniot relations are used to deduce the pressure p_s at the shock front from the measured shock velocity, u_s, and the density, ρ_s, at the shock front using $p_s = p_0 + \rho_0 [1 - \rho_0/\rho_s] (u_s)^2$ where ρ_0 is the unshocked density and p_0 is the pressure in the unshocked material.

Using the shock tracker, we can extract the Hugoniot data from the simulations. Figure 5 plots the pressure vs density from the simulation (red curve) and compares it with the Hugoniot (black curve) from LEOS 5400 table used in the calculation. One notices excellent agreement between the experiment and theory within 0.2% over the entire pressure range of 50-130 Mbar which gives us great confidence that the experiment is a valid method for measuring Hugoniot data even though we have a converging shock. Locally the shock acts as a series of planar shock allowing one to extract a locus of Hugoniot data from a single experiment. We developed a method to smooth out the noise in the Hugoniot data extracted from the simulation by dividing the density versus pressure curve by the table Hugoniot, fitting the result to a fourth order polynomial over the range of interest and then multiplying by the divisor of the previous ratio. To understand the effect of preheat for the low drive experiment we redid the calculation using an equivalent black body radiation source that does not have the Au M-shell in the detailed frequency dependent spectrum. If we use the fraction of radiation above 1.9 keV as a metric for the "M-shell" radiation our frequency dependent

source has 1.6% of radiation above 1.9 keV while the equivalent black body source only has 0.2%. However, the Hugoniot data we extract using the temperature source looks virtually identical to that from the frequency dependent source indicating that preheat is not an issue for the low-drive experiments. To quantify the effect of self-emission from the shock front we redid the simulation zeroing out the emission and absorption opacity for the unshocked material in front of the shock. This eliminates the effect of the self-emission from the shock heating any material in front of the shock. Again, the Hugoniot we extract from the simulation does not change indicating that self-emission is not an issue for the low-drive experiments that measure data up to a pressure of 130 Mb.

If we now look at the high-drive experiments, the simulations predict that the shock reaches the boundary of the CH at 3.15 ns with an ablation pressure of 94 Mbar. The shock continues to travel inward and starts to slowly increase as seen in Fig. 6. where we plot the shock pressure vs position of the shock front. Table 2 shows a shock pressure of 130 Mbar at a radius of 800 μm and time of 4.58 ns that slowly increases to 373 Mb as the shock reaches a radius of 200 μm at 8.35 ns. Between 200 and 100 μm the pressure starts to climb more rapidly from 373 to 638 Mb as the shock reaches 100 μm at t=8.76 ns. As the shock continues to accelerate inward to the center the pressure doubles to over 1.1 Gbar in the next 160 ps as the shock reaches a radius of 49 μm. Experimentally it becomes hard to measure the shock with adequate resolution below a radius of 100 μm. It is also important to point out that the opacity of the CH plastic at the 9 keV energy of the backlighter used in the experiments decreases to half of the cold opacity by a pressure of 400 Mb. As the Gbar EOS experiments reach the higher pressures that enable one to see K-shell effects [7] on the Hugoniot, these are also the conditions where K-shell ionization causes the opacity used in the radiographic unfold of the density to change significantly from the cold opacity values. The opacity effects will be discussed in a separate paper.

Figure 7 plots the pressure vs density from the simulation (red solid) and compares it with the Hugoniot data from the LEOS 5400 table (black solid) used in the calculation. One can see that the simulation has a lower density even at the lowest pressures near 100 Mb. To understand this, we also plot a series of Hugoniots (black dotted) with initial temperatures that vary from 1 – 5 eV with the 1 eV curve being closest to the nominal Hugoniot. One can now see that the simulated Hugoniot starts at an effective temperature between 3 and 4 eV which is due to preheat from the hohlraum source. After the laser drive turns off the preheat starts to decrease and the simulation initially moves closer to the baseline Hugoniot. As the pressure climbs above 300 Mb the density

starts to bend to lower densities due to the self-emission from the shock front heating the un-shocked material.

To understand the effect of preheat for the high-drive experiment we redid the calculation using an equivalent black body radiation source that does not have the Au M-shell in the detailed frequency dependent spectrum. Using the fraction of radiation above 1.9 keV as a metric for the "M-shell" radiation our frequency dependent source has 10.4% of radiation above 1.9 keV while the equivalent black body source only has 4.9%. While this reduces the preheat it does not eliminate it as seen in the blue solid curve in Fig. 8 which shows the simulated Hugoniot using this temperature source. The effective temperature is now between 1 and 2 eV.

To eliminate both the preheat from the hohlraum as well as the self-emission from the shock front we redid the simulation zeroing out the emission and absorption opacity for the un-shocked material in front of the shock as shown by the green dotted curve in Fig. 8. To do this simulation we first identified the shock front and then zeroed out the opacity only in the unshocked material at each time step in the simulation. By zeroing out the opacity, the unshocked material does not absorb radiation and is not heated by any of the X-rays emitted in the hot plasma at and behind the shock front. In this case the simulation nicely follows the Hugoniot curve up to pressures of 400 Mb and above. It does slightly drift to higher density but even at 700 Mb the density is only 1% above the Hugoniot value. Showing that we understand how to remove the effect of preheat and self-emission in the simulations gives us more confidence in our ability to model and quantify these effects.

Based on these calculations, for the actual Gbar experiments using a PAMS target, we decided to limit our Hugoniot data to a pressure of about 400 Mb even though the experimental data goes to 650 Mb at the minimum radius of 100 μm.

To illustrate the effect of preheat we look at lineouts of the temperature and density at a time of 5.0 ns in the high-drive simulation, which is the peak of the laser drive and the preheat. The shock pressure is 145 Mbar. Figure 9 plots the electron temperature vs radius when the shock is at 744 μm for the nominal simulations (red solid) that include the effects of preheat as compared with the case (black solid) when we zero out the opacity in front of the shock to eliminate radiation effects on the Hugoniot. One observes that the temperature in front of the shock is about 4 eV when the preheat is included, which is consistent with the Hugoniot values we extract from the simulation in Fig. 7. To see the effect the preheat has on the density Fig. 10 plots density vs radius for these two cases. One notices that the density is 2% lower for the red curve that includes the effects of

preheat.

To better understand the challenges with this type of experiment and why the simulations are drifting to low density from the self-emission we look at lineouts of the temperature, pressure, and density at a time of 8.8 ns in the high-drive simulation. Figure 11 shows the pressure vs radius near the shock front when the shock is at 89 μm for the nominal simulations (red solid) that include the effects of preheat and self-emission as compared with the case (black solid) when we zero out the opacity in front of the shock to eliminate radiation effects on the Hugoniot. One notices that the pressures are similar within 5% while the electron temperature, shown in Fig. 12, has a significant rise near the shock front and falls off rather slowly in front of the shock when the full simulation with radiation is included. The temperature exceeds 50 eV in the un-shocked material. Figure 13 plots the density vs radius and one can see how the self-emission rounds off the sharp jump in the density and makes the density at the shock front about 18% lower even though the overall shape of the density curves are very similar behind the shock. The self-emission is causing a very substantial heating of the un-shocked material and driving the experiment off of the Hugoniot curve. In future experiments, it would be interesting to try to directly measure the effect of radiative heating on the Hugoniot.

4. Conclusions

For the low-drive Gbar EOS experiments using CH targets the simulations show that the shock front lies nicely on the Hugoniot over the pressure range of 40 – 130 Mbar and that the effects of radiation pre-heat and self-emission from the shock front do not have any significant effect on the Hugoniot measurements. The simulations also give us confidence that the shock front for the converging geometry Gbar EOS experiments are indeed on the Hugoniot. The situation is quite different for the high drive Gbar simulations. In this case we show how the high energy x-rays from the hohlraum pre-heat the unshocked material and cause the experiment to lie on a pre-heated Hugoniot with temperatures near 3-4 eV at early times. As the shock converges toward the center we show how the self-emission from the shock front starts to heat the unshocked material even more and drives the experiment further off the Hugoniot. Using the 5% uncertainty in the experimental measurement of the density as a benchmark we conclude that the effects of self-emission start becoming a significant effect above pressures of 400 Mb.

Acknowledgements. This work was performed under the auspices of the U.S. Department of

Energy by Lawrence Livermore National Laboratory under Contract DE-AC52-07NA27344.

References

[1] L. Stixrude, Phys. Rev. Lett. 108 (2012) 055505.
[2] S. Seager, et al., Astrophys. J. 669 (2007) 1279.
[3] V. E. Fortov, Extreme States of Matter on Earth and in the Cosmos, Springer-Verlag, Heidelberg, 2011, p. 224.
[4] A. L. Kritcher, T. Döppner, D. Swift, J. Hawreliak, G. Collins, J. Nilsen, B. Bachmann, E. Dewald, D. Strozzi, S. Felker, O.L. Landen, O. Jones, C. Thomas, J. Hammer, C. Keane, H.J. Lee, S. H. Glenzer, S. Rothman, D. Chapman, D. Kraus, P. Neumayer, R.W. Falcone, "Probing matter at Gbar pressures at the NIF," HEDP **10**, 27 – 34 (March 2014).
[5] T. Döppner, D. C. Swift, A. L. Kritcher, B. Bachmann, G.W. Collins, D.A. Chapman, J. Hawreliak, D. Kraus, J. Nilsen, S. Rothman, L. X. Benedict, E. Dewald, D. E. Fratanduono, J. A. Gaffney, S. H. Glenzer, S. Hamel, O. L. Landen, H. J. Lee, S. LePape, T. Ma, M.J. MacDonald, A. MacPhee, D. Milathianaki, M. Millot, P. Neumayer, P. A. Sterne, R. Tommasini, R. W. Falcone, "Absolute equation-of-state measurements for polystyrene from 25 - 60 Mbar using a spherically converging shock wave," Phys. Rev. Lett. (July 9, 2018).
[6] Damian C. Swift, Andrea L. Kritcher, James A. Hawreliak, Amy Lazicki, Andrew MacPhee, Benjamin Bachmann, Tilo Döppner, Joseph Nilsen, Gilbert W. Collins, Siegfried Glenzer, Stephen D. Rothman, Dominik Kraus, and Roger W. Falcone, "Absolute Hugoniot measurements from a spherically-convergent shock using x-ray radiography," Rev. Sci. Instr. **89**, 053505 (May 18, 2018).
[7] Andrea L. Kritcher et al., "Laboratory equation of state measurements of carbon atmospheres of white dwarf stars," LLNL report LLNL-xxxxxx (July 2019).
[8] M. Rosen *et al.*, High Energy Density Phys. **7** (2011) 180-190.
[9] G. B. Zimmerman and W. L. Kruer, comments in Plasma Physics and Controlled Fusion **2**, 51-61 (1975).
[10] M. K. Nemanic and P. Nowak. Radiation transport calculations on unstructured grids using a spatially decomposed and threaded algorithm. In *Mathematics and Computation, Reactor Physics and Environmental Analysis in Nuclear Applications*, Madrid (ES), April 1999.
[11] P. G. Maginot, P. F. Nowak, and M. L. Adams. A review of the upstream corner balance spatial discretization. In *International Conference on Mathematics and Computational methods, Applied to Nuclear Science and Engineering*, Jeju, Korea, April 2017.

Table 1. Pressure at shock front vs time and radius for low-drive Gbar simulation		
Time	Radius	Pressure
8.85	600	39
10.27	500	40
11.64	400	45
12.91	300	54
14.04	200	73
14.96	100	132

Table 2. Pressure at shock front vs time and radius for high-drive Gbar simulation		
Time	Radius	Pressure
4.58	800	130
5.33	700	155
6.02	600	181
6.67	500	208
7.27	400	235
7.84	300	280
8.35	200	373
8.76	100	638
8.85	74	807
8.92	49	1122

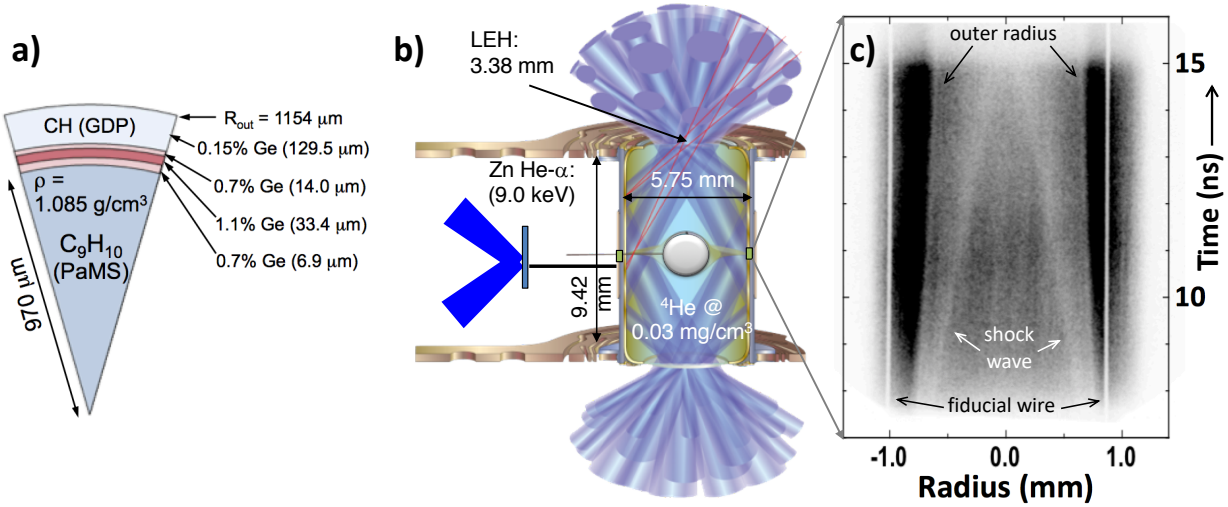

Fig. 1. a) Schematic of the solid spherical CH target with Ge doped GDP ablator used on the Gbar experiments. b) Schematic of the experimental setup. Solid spherical target of CH is shock compressed using a hohlraum radiation drive, then backlit with ~9 keV Zn He-α X-rays to generate a time-resolved ("streaked") 1D image of the shock compression vs time. c) Radiograph for the 9 keV X-ray backlighter versus time and radius showing the shock wave converging to the central hot-spot. The vertical axis covers 8 ns and the horizontal axis covers a diameter of 0.2-cm. Details of experiment are in Ref. 5.

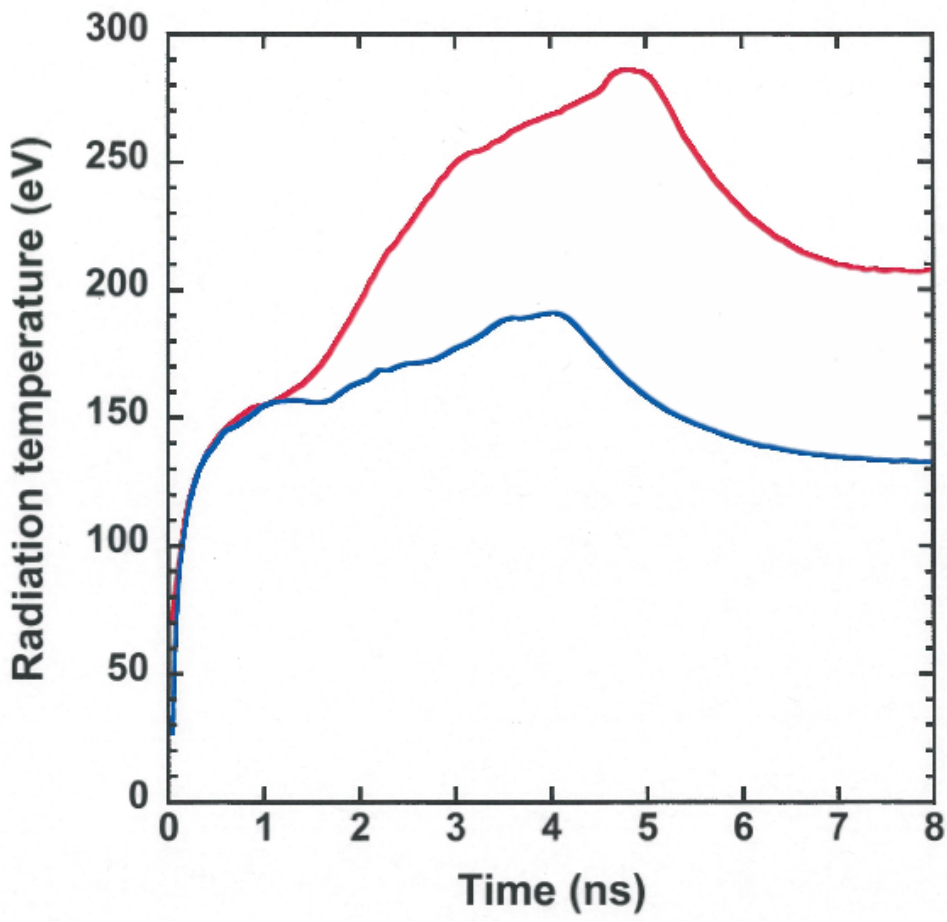

Fig. 2. Simulated radiation temperature versus time inside the radiation cavity (hohlraum) comparing the cases for high (red) and low-drive (blue) Gbar experiments.

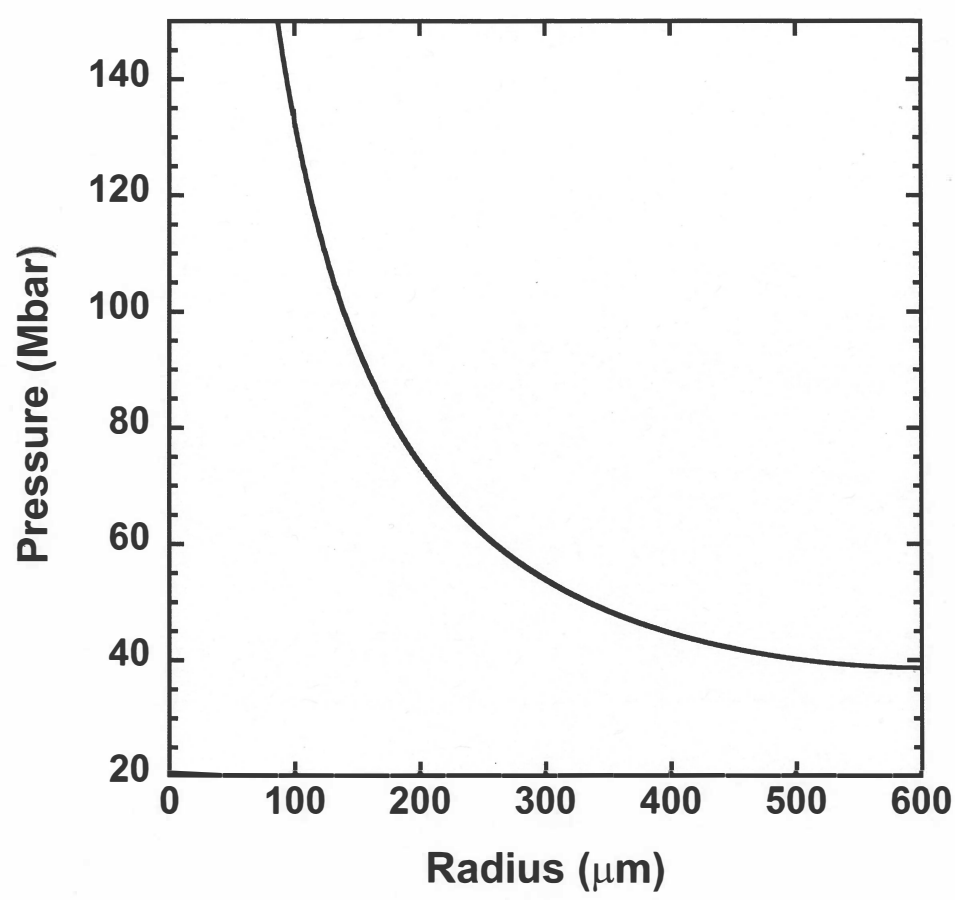

Fig. 3. Pressure at the shock front vs shock radius for the low-drive Gbar simulations of a solid CH target. One can see how the pressure starts increasing steeply as the shock converges to radii less than 200 μm.

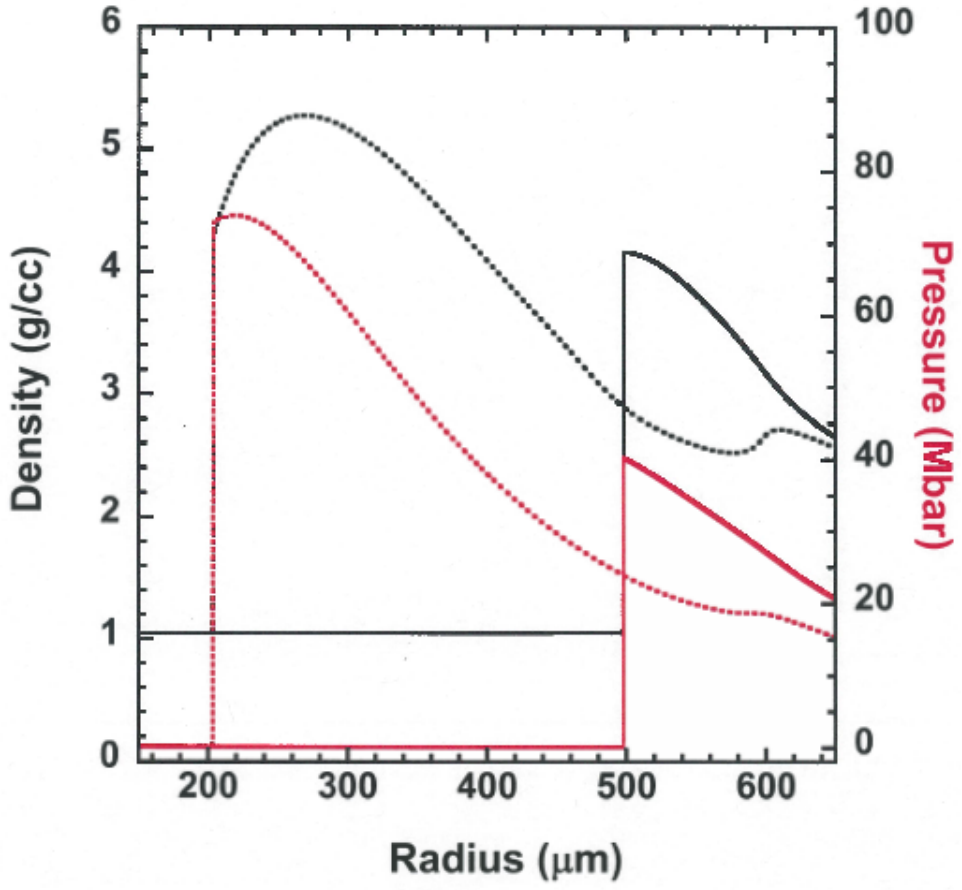

Fig. 4. Snapshots of the simulated density (black) and pressure (red) versus radius of the CH spherical target for the low-drive Gbar simulations at 10.3 and 14.0 ns. At early time and large radius (solid) the pressure and density peak at the shock front. As the shock converges toward the center (dotted) there is a significant pileup in the density behind the shock.

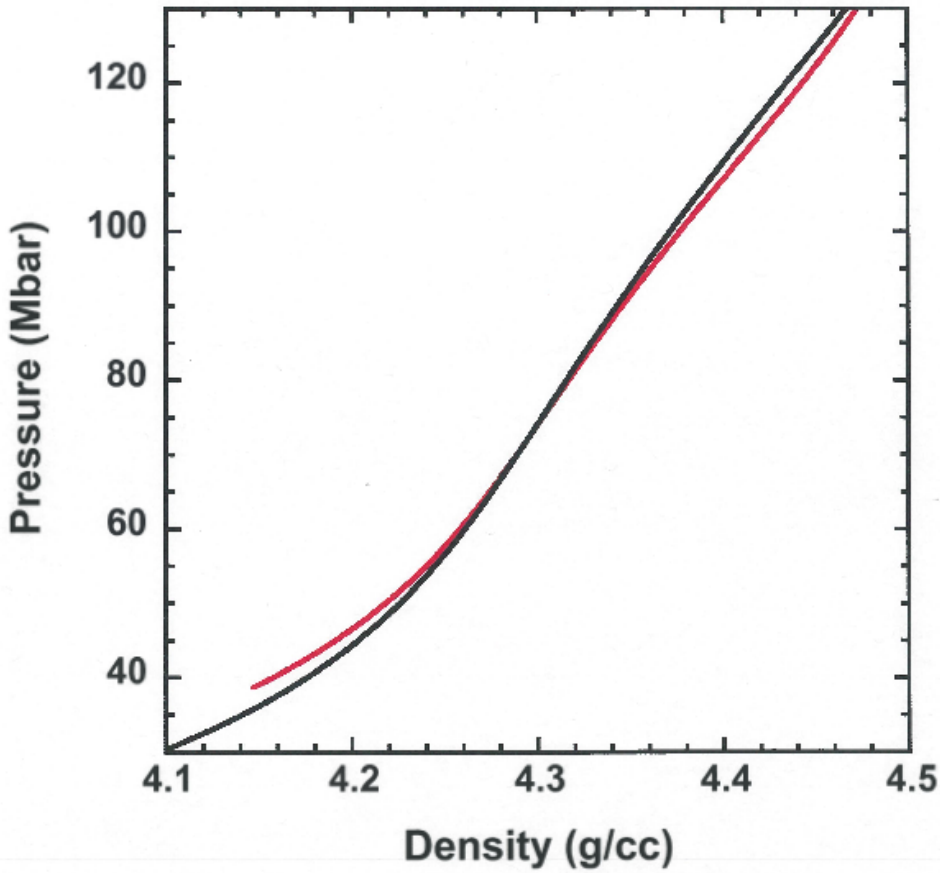

Fig. 5. The solid black line shows the pressure vs density for the Hugoniot from tabular EOS table LEOS 5400. The red curve is the values of pressure and density extracted from the radiation-hydrodynamic simulations for the low-drive Gbar simulation of a solid CH target. There is excellent agreement within 0.2% over the pressure range of 50-130 Mbar.

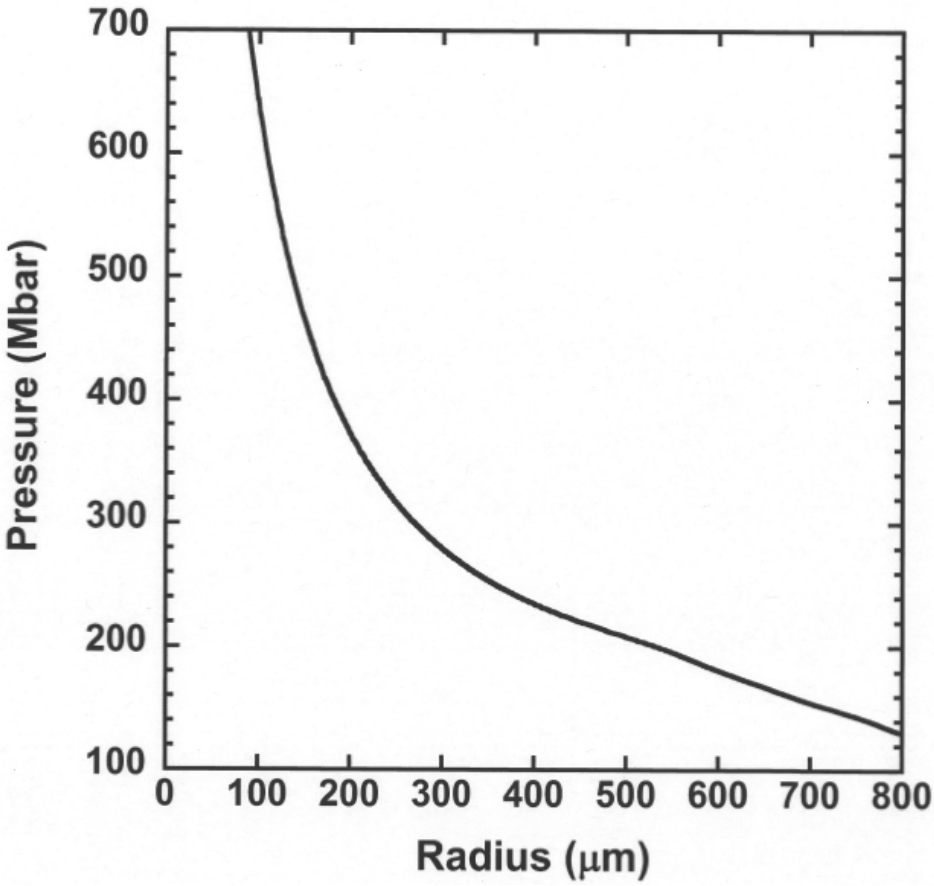

Fig. 6. Pressure at the shock front vs shock radius for the high-drive Gbar simulations of a solid CH target. One can see how the pressure starts increasing steeply as the shock converges to radii less than 200 μm.

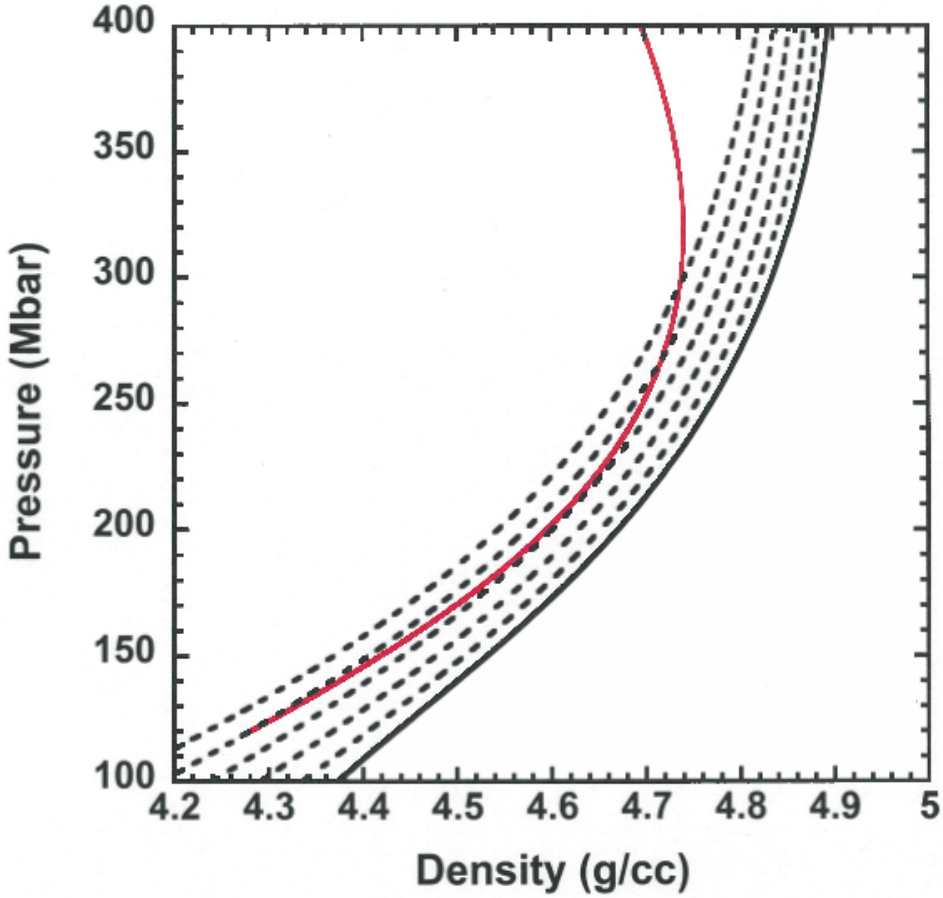

Fig. 7. The solid black line shows the pressure vs density for the Hugoniot from tabular EOS table LEOS 5400. The dotted lines are the Hugoniot for LEOS 5400 with initial temperatures from 1 – 5 eV with 1 eV being closest to the solid curve. The red curve is the values of pressure and density extracted from the radiation-hydrodynamic simulations for the high-drive Gbar simulation of a solid CH target. The simulation initially lies on a preheated Hugoniot between 3 and 4 eV.

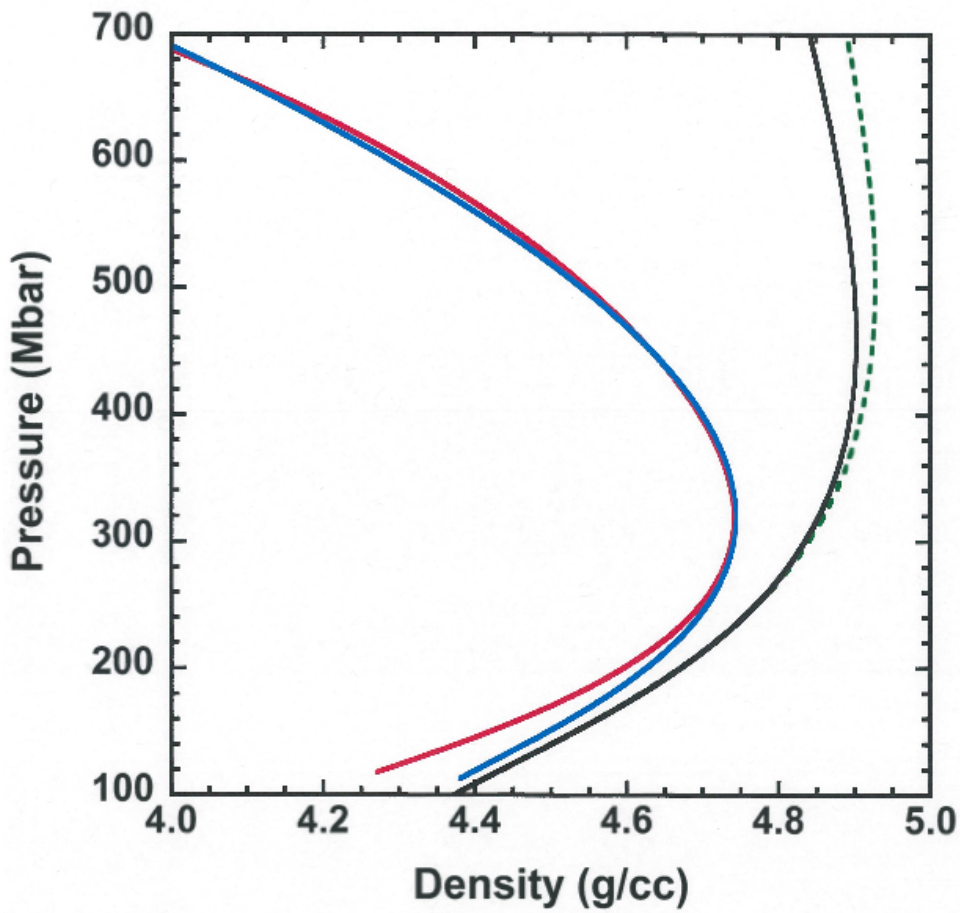

Fig. 8. The solid black line shows the pressure vs density for the Hugoniot from tabular EOS table LEOS 5400. The red curve is the values of pressure and density extracted from the radiation-hydrodynamic simulations using the full FDS source for the high-drive Gbar simulation of a solid CH target. The blue curve uses an equivalent black body source to drive the CH target while the green dotted curve uses the full FDS source but zeroes out the opacity in front of the shock to eliminate the effects of pre-heat and radiative heating from the shock on the unshocked material.

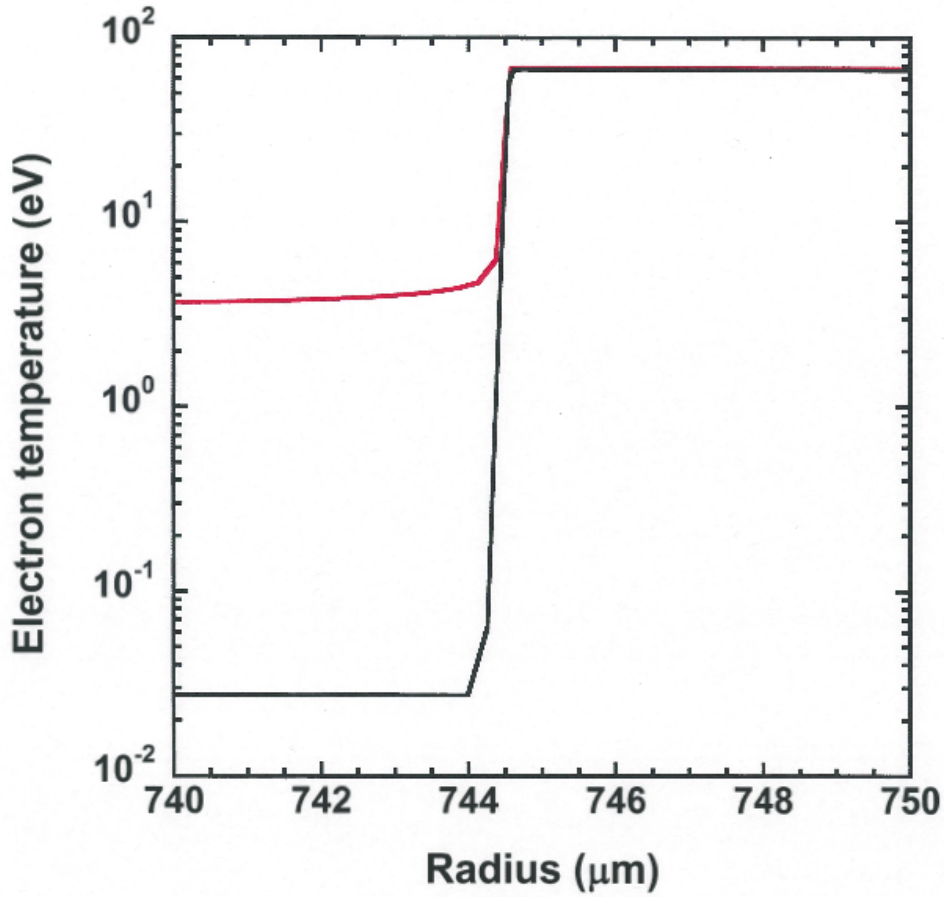

Fig. 9. Snapshots of the simulated electron temperature versus radius of the CH spherical target for the high-drive Gbar simulations when shock reaches 744 μm radius at time 5.0 ns. The red curve is the baseline simulation using the full FDS source while the black curve is the same simulation with the opacity zeroed out in front of the shock to eliminate the radiation heating effects. The radiative heating from the preheat heats the unshocked material to temperatures of about 4 eV in front of the shock.

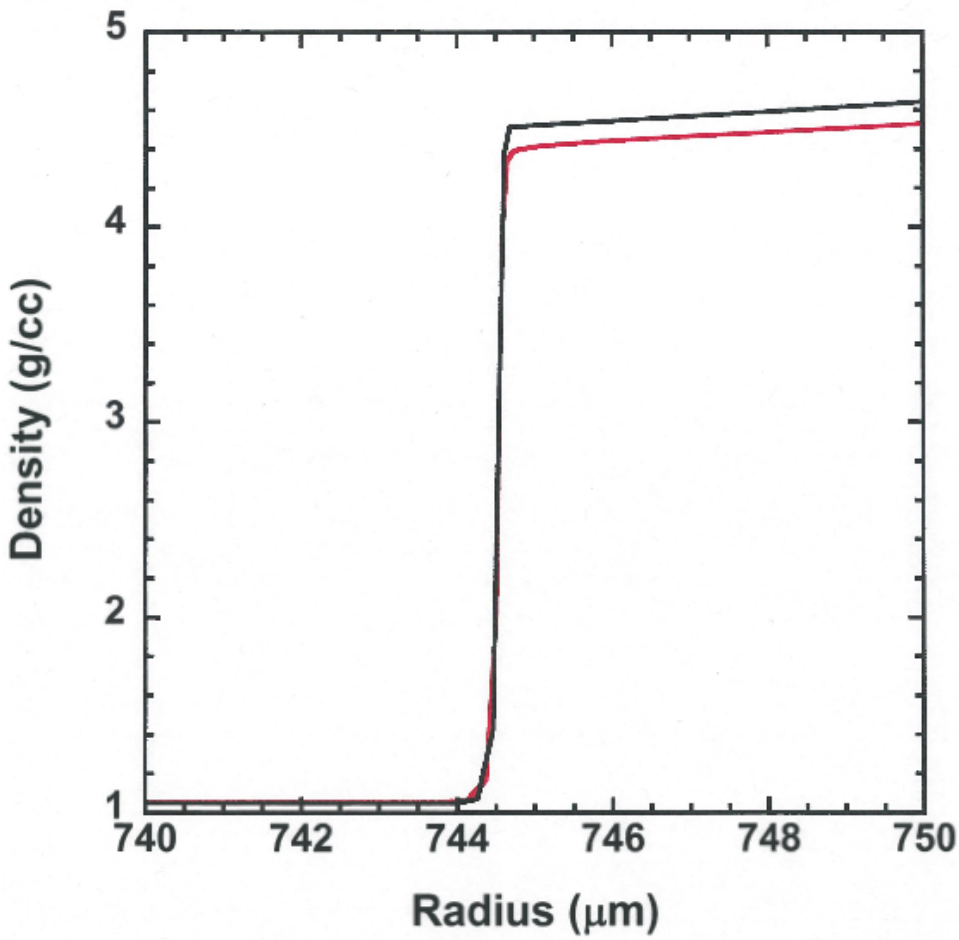

Fig. 10. Snapshots of the simulated density versus radius of the CH spherical target for the high-drive Gbar simulations when shock reaches 744 μm radius at time 5.0 ns. The red curve is the baseline simulation using the full FDS source while the black curve is the same simulation with the opacity zeroed out in front of the shock to eliminate the radiation heating effects. The density is about 2% lower in the preheated case.

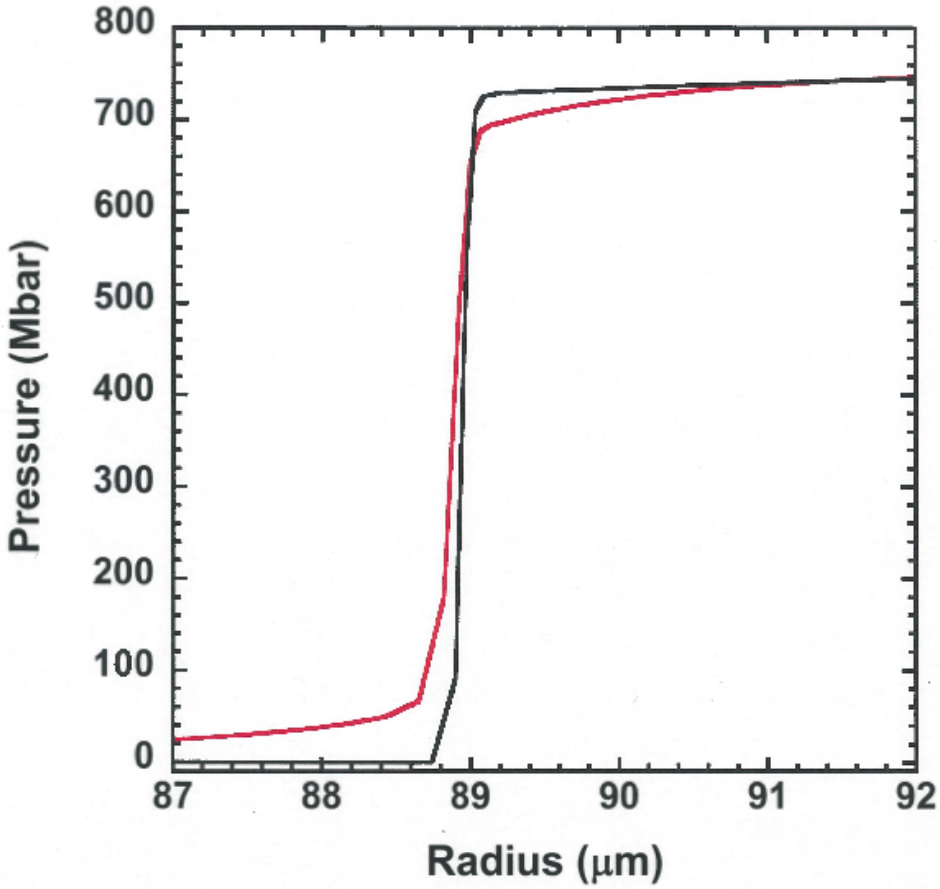

Fig. 11. Snapshot of the simulated pressure versus radius of the CH spherical target for the high-drive Gbar simulations when shock reaches 89 μm radius at time 8.8 ns. The red curve is the baseline simulation using the full FDS source while the black curve is the same simulation with the opacity zeroed out in front of the shock to eliminate the radiation heating effects.

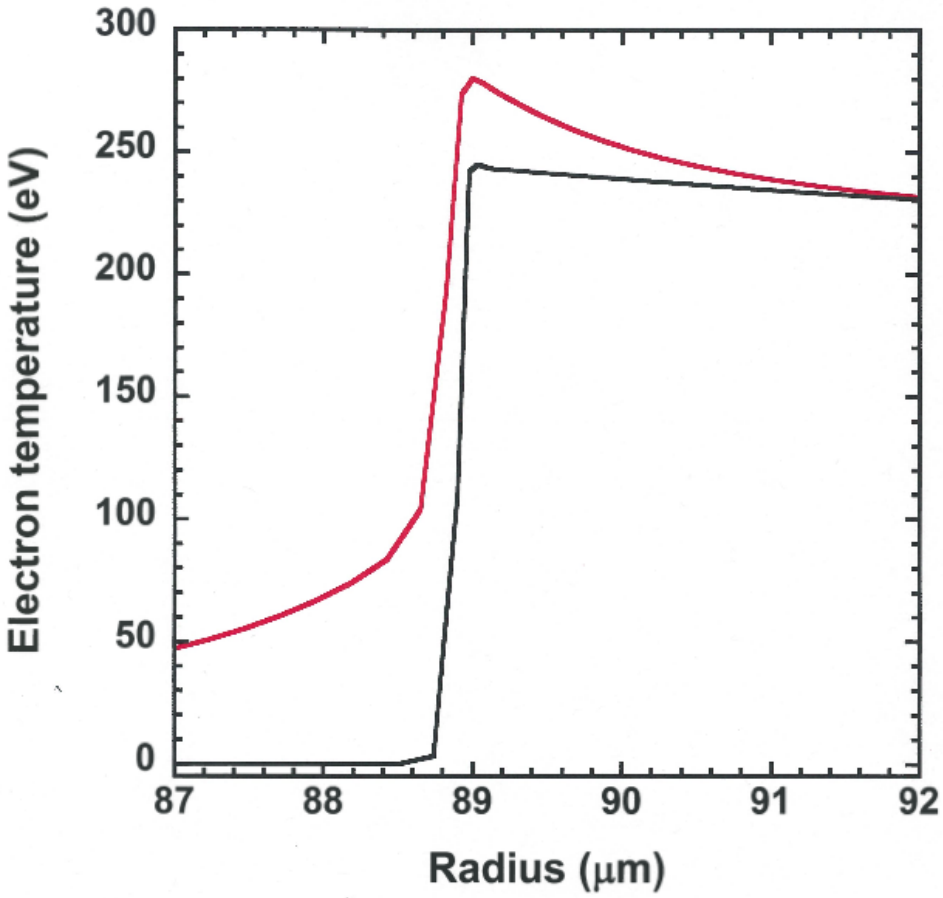

Fig. 12. Snapshots of the simulated electron temperature versus radius of the CH spherical target for the high-drive Gbar simulations when shock reaches 89 μm radius at time 8.8 ns. The red curve is the baseline simulation using the full FDS source while the black curve is the same simulation with the opacity zeroed out in front of the shock to eliminate the radiation heating effects. The radiative heating from the shock heats the unshocked material to temperatures exceeding 50 eV in front of the shock.

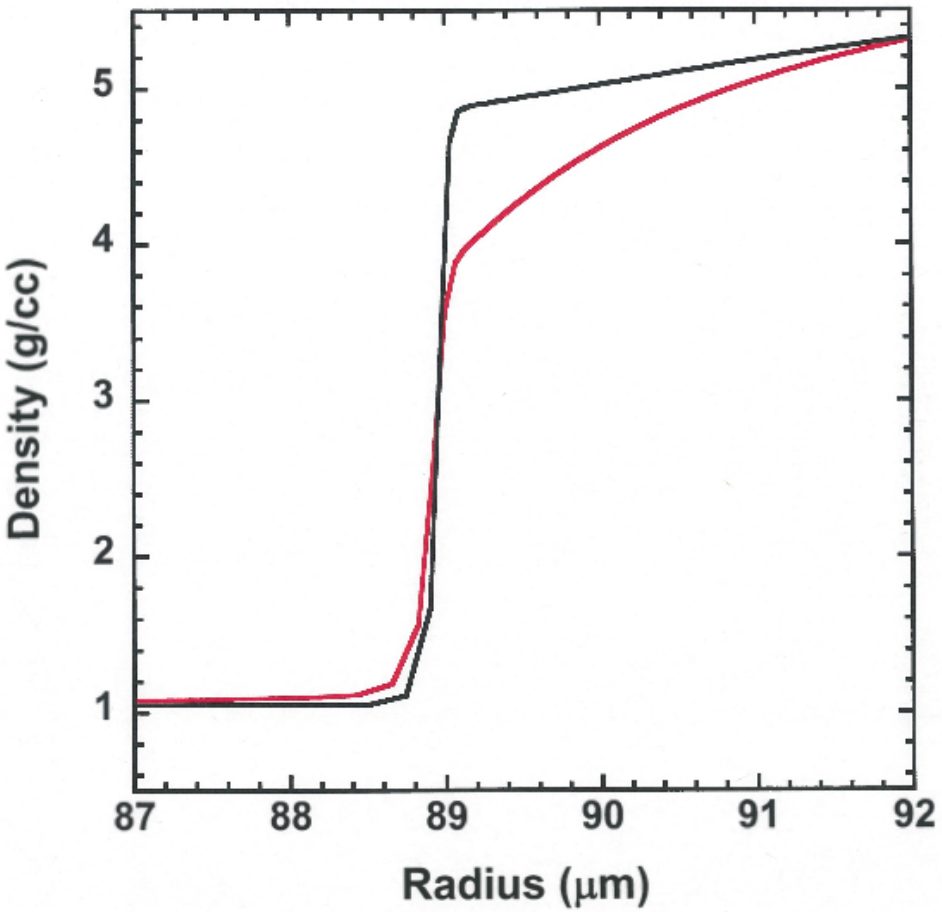

Fig. 13. Snapshots of the simulated density versus radius of the CH spherical target for the high-drive Gbar simulations when shock reaches 89 μm radius at time 8.8 ns. The red curve is the baseline simulation using the full FDS source while the black curve is the same simulation with the opacity zeroed out in front of the shock to eliminate the radiation heating effects. The density has dropped significantly at the shock front due to radiative heating.